Transverse dynamics of water across the melting point: A parallel neutron and x-ray inelastic scattering study

A. Cunsolo, C. N. Kodituwakku, F. Bencivenga, M. Frontzek, B. M. Leu, and A. H. Said

Phys. Rev. B **85**, 174305 — Published 29 May 2012

DOI: 10.1103/PhysRevB.85.174305

Transverse dynamics of water across the melting: a parallel Neutron and X Ray Inelastic Scattering study

A. Cunsolo and C. N. Kodituwakku

Brookhaven National Laboratory-National Synchrotron Light Source-II,

P.O. Box 5000 Upton, NY, 11973, USA

F. Bencivenga

Sincrotrone Trieste, S.S. 14 km 163,

5 in AREA Science Park 34012 Basovizza, Trieste, Italy

M. Frontzek

Neutron Scattering Science Division,

Oak Ridge National Laboratory,

Oak Ridge, TN 37831, USA

B. M. Leu and A. H. Said

Advanced Photon Source, Argonne National Laboratory,

Chicago, IL, 60439 USA

(Dated: April 24, 2012)

Joint Inelastic Neutron and X Ray Scattering measurements have been performed on heavy water across the melting point. The spectra bear clear evidence of a low and a high frequency inelastic shoulders related to a transverse and a longitudinal mode, respectively. Upon increasing the momentum transfer, the spectral shape evolves from a viscoelastic regime, where the low frequency mode is clearly over-damped, towards an elastic one where its propagation becomes instead allowed. The crossover between the two regimes occurs whenever both the characteristic frequency and the line-width of the low frequency mode match the inverse of the structural relaxation time. Furthermore, we observe that the frequency of the transverse mode undergoes a discontinuity across the melting, whose extent reduces upon increasing the exchanged momentum.

PACS numbers: 62.60.+v,34.50.-s,73.21.-b,25.40.Fq

I. INTRODUCTION

The presence of a second, low-frequency and weakly dispersing mode in the THz spectrum of water is a common finding of several Inelastic Neutron[1–4] and X Ray[5–9] Scattering (*INS* and *IXS* respectively) experiments. Its onset was at first predicted in the mid-1970s by a molecular dynamics (MD) simulation[10] and more recently interpreted, by similar computational methods, as the manifestation of a THz viscoelastic behavior[11]. This low-frequency excitation appears in the spectrum of density fluctuations , $S(Q,\omega)$, when the exchanged momentum, Q, exceeds some threshold value, $Q_T \approx 4\ nm^{-1}$, and, according to a broadly accepted interpretation[7–9,11], it arises from the coupling of density fluctuations with shear waves[12]. This explanation stems from the analogy with ice, whose spectrum is characterized by an optic transverse phonon at comparable frequencies[13]. Furthermore, it is supported by MD results[8,11] demonstrating the presence of an analogous peak in the correlation function of transverse velocities.

In summary, the body of literature results on the $S(Q,\omega)$ of water outlines a rather coherent scenario: owing to the lack of translational invariance typical of liquids, longitudinal and transverse modes become mutually intertwined and their symmetry somehow ill-defined at distances shorter than some threshold $\approx Q_T^{-1}$. Such longitudinal-transverse (L-T) coupling causes the onset of an inelastic transverse mode in the $S(Q,\omega)$, even if the latter, in principle, only couples with longitudinal modes.

It seems natural to ascribe the strength of the L-T coupling in water to the presence of a hydrogen bond network, which enhances the correlations between the movements of molecules belonging to adjacent layers of the liquid, thus fostering the propagation of shear waves. An L-T coupling has been demonstrated in other simulated network systems such as glassy glycerol[14] and also experimentally observed in SiO_2[15], GeO_2[16] and $GeSe_2$[17], samples sharing with water the property of a tetrahedral arrangement of local intermolecular structure. The circumstance that L-T coupling was evidenced experimentally only in tetrahedrally arranged systems suggests that this peculiar symmetry of the local structure somehow fosters this effect. Most important, both the Q and the temperature, T, dependencies[8] suggest that the onset of the transverse mode has a precursor in the viscoelastic transition of the longitudinal sound velocity[18], induced by the presence of a structural relaxation process. The physical link between these effects becomes clear as one reckons that the viscoelastic crossover mainly reveals the evolution from the viscous, liquid-like,

response to the elastic, solid-like, one. The propagation of shear waves, albeit forbidden in the viscous limit, becomes in principle allowed when the solid like one is reached. The crossover frequency between these two regimes is defined by the inverse of the structural relaxation time, $1/\tau$. In this respect, in Ref. 8 it is convincingly shown that the transverse mode shows up only when its frequency, Ω_t, overtakes $1/\tau$. Furthermore, it has been experimentally demonstrated that the strength of the L-T coupling enhances either by increasing Q or by decreasing T[8]. Upon increasing Q, one eventually probes distances shorter than the typical size of the structural relaxation, λ_s. On the other hand, upon decreasing T, both τ and λ_s increase, which makes the elastic regime observable at lower Q values, or, correspondingly, over greater distances. In this regime the liquid dynamics becomes similar to the one of the solid, i.e. characterized by a higher sound velocity, a lower sound damping and the onset of transverse propagation.

From this perspective, it would be presently of great interest to investigate the evolution of the L-T coupling upon approaching (and crossing) the melting point. Unfortunately, the two spectroscopic techniques best suited to this purpose, INS and IXS, suffer from inherent limitations hampering the achievement of this goal. In fact, from one side, state-of-art IXS spectrometers have a rather broad and slowly decaying resolution function, often unfit to properly resolve the low frequency peak. Conversely, INS instruments can be operated with extremely narrow (sub-meV broad) and sharp, nearly Gaussian, resolution function, yet only at the expense of a narrowing of the spanned dynamic range.

Based upon the above arguments, we decided to take advantage of the complementarity of these two techniques to attempt a joint study of the spectral shape of deuterated water, D_2O, by lowering T. The simultaneous use of the two probes allowed us to measure the spectral shape of water with unprecedented narrow resolution bandwidth (0.1 meV) and over a rather large energy transfer range $E \leq 40meV$ (here $E = \hbar\omega$, with $\hbar$ being the Plank's constant over 2π). The reason for using D_2O, rather than H_2O, is the much higher coherent-to-incoherent cross section ratio of deuterium as compared to hydrogen, which allows one to achieve a reliable measurement of $S(Q,\omega)$.

We end this introductory section with a brief note: although the main effect of both the local disorder and the L-T coupling is destroying the pure symmetry of the inelastic modes, hereafter we will still quote the high- (low-) frequency inelastic peak of $S(Q,\omega)$ to as the longitudinal (transverse) peak, as it basically corresponds to the dominating mode in the longitudinal (transverse) current spectra[11].

II. THE EXPERIMENT

The instrument used to collect neutron spectra was the new Cold Neutron Chopper Spectrometer (CNCS) operating at the Spallation Neutron Source (SNS) of Oak Ridge National Laboratory, TN. It is a direct geometry, multi-chopper, inelastic spectrometer optimized for incident neutron energies included between 2 and 50 meV, thus providing a high flexibility in the choice of the energy resolution[19]. The latter was measured with 3.7 meV incident neutron energy using a vanadium standard and it was found to be 0.1 meV broad (Full-Width-at-Half-Maximum, FWHM) and essentially Gaussian in shape.

The D_2O sample was contained inside an aluminium slab, whose thickness (0.5 mm) represented a reasonable compromise between the conflicting needs of enhancing the sample signal and limiting the multiple scattering. The sample container was inserted into the internal chamber of an Orange cryostat[20] and therein kept at the desired temperature, within a $\pm 0.01K$ stability.

Each determination of the (Q, ω) surface typically took 2 hours acquisition time. Once achieved, the constant Q spectra were extracted by interpolation at nine Q values spanning the 6-24 nm^{-1} range, which includes the First Sharp Diffraction Peak (FSDP) of the D_2O sample ($\approx 19.5\ nm^{-1}$).

The IXS measurements were carried out at the HERIX spectrometer of the Sector 30 beamline at the Advanced Photon Source (Argonne National Laboratory). The energy of the incident beam was tuned to $\approx 23.7\ keV$, corresponding to the *Si(12 12 12)* backscattering reflection from the spherical analyzers. The photons scattered by the sample were energy analyzed by 9 independent analyzers mounted on the tip of a rotating arm and mutually separated by the same Q offset, $\Delta Q = 2\ nm^{-1}$. The spectrometer angle was chosen to probe in a single energy scan the 2-18 nm^{-1} Q-range. The beam impinging on the sample had a 35x15 μm^2 (horizontal x vertical, FWHM) focal spot. The instrumental resolution function was evaluated through the measurement of the spectral shape from an almost elastic scatterer, i.e. Plexiglas, at the Q of its FSDP ($Q_m \approx 14\ nm^{-1}$). It was found to have a pseudo-Voigt shape with nearly 1.6 meV FWHM, thus being narrow enough to properly resolve the high frequency peaks of water all over the spanned Q-range. Further details on the spectrometer can be found elsewhere[21,22].

Raw INS spectra were corrected for the intensity scattered by the empty sample container. This scattering intensity was measured with the same integration time as the raw spectrum and then subtracted from it after a

proper account of calculated transmissions. Furthermore, the incoherent scattering line-shape was subtracted from INS spectra, as estimated using the Sears model[23] of rotational diffusion spectrum. The latter was evaluated using the rotational diffusion coefficient reported in Ref. 24, while adjusting the integrated intensity so as to satisfy $\sigma_{INC}/(\sigma_{COH} + \sigma_{INC}) = 0.21$, where σ_{INC} and σ_{COH} are the total incoherent and the coherent extinction cross sections respectively, given by the sum of their absorption and scattering components. When performing the data reduction, in principle, the dependence of the extinction cross sections on the incident neutron energy (E_i) should have been taken into account. However, since the transmission is very close to 1, the E_i-dependence of the cross sections can be safely neglected. Unfortunately, to the best of our knowledge, no multiple scattering, MS, calculations on D_2O is available in literature in the dynamic region and for scattering geometries considered in the present INS experiment. However, previous Monte Carlo calculation of the double scattering performed by some colleagues[25] shows that, although MS can be as high as 6% the of single scattering intensity, its energy profile is flat enough to be reasonably approximated by a constant plateau[26]. Indeed, when fitting the spectra, MS contamination was accounted for by a flat background parameter in the model function. Concerning the influence of MS on the fitting results (to be discussed in the following), some further comment is here needed. In principle a poor knowledge of the MS shape would unavoidably produce less than reliable fitting results, especially considering the relevance of MS intensity in the region of INS spectral tails. On the other hand, this spurious intensity should not dramatically affect the evaluation of both positions and line-width of the low frequency peak, which is the main focus of this work. Conversely, MS can in principle affect the determination the relaxation timescale τ to be discussed further below. However the comparison between the τ values obtained best fitting INS spectra and the ones derived from fitting IXS intensities (mostly unaffected by multiple scattering, as discussed in Ref. 18) suggests that multiple scattering effects, if sizable, do not dramatically influence the measured Q and T-dependencies of fitting results.

For IXS spectra, the essentially flat background level was only marginally due to the rather low ($< 1\ mHz$) electronic noise of detectors, it was rather dominated by the scattering coming from both the Kapton windows of the sample container and the Be dome surrounding it. Its profile mainly consisted of a rather intense plateau with a weak central peak atop, as narrow as the resolution and essentially negligible when compared to the sample signal. Although no attempt was made to subtract such background from raw IXS spectra, a frequency independent term has been used to account for it when modeling the best fit line-shapes (see Eq. 6 further below).

Neutron spectra were collected in a broad T region including the liquid-solid transition ($268\ K \leq T \leq 305\ K$)

while IXS measurement covered a slightly narrower T region (288 $K \leq T \leq$ 307 K).

III. THEORETICAL BACKGROUND

The observable measured by IXS experiments is the spectrum of density fluctuations, $S(Q,\omega)$, usually referred to as dynamic structure factor. This variable is simply related to the spectrum of longitudinal current correlation function, $C_l(Q,\omega)$, through[27]:

$$C_l(Q,\omega) = (\omega/Q)^2 S(Q,\omega). \tag{1}$$

The variable $C_l(Q,\omega)$ is also called the current spectrum and is defined as the Fourier transform of:

$$C_l(Q,t) = 1/N\langle J_Q^*(Q,0) J_Q(Q,t)\rangle. \tag{2}$$

Here we introduced the longitudinal current variable $\mathbf{J}_Q(Q,t) = \sum_j \mathbf{v}_{Q,j}(t) \exp -i\mathbf{Q}\cdot\mathbf{r}_j(t)$, where $\mathbf{r}_J(t)$ and $\mathbf{v}_{Q,j}(t)$ are the position of j-th molecule and the projection along $\hat{\mathbf{Q}}$ of its velocity, respectively, while the index "j" runs over all molecules in the system. When the L-T mixing occurs[28], $C_l(Q,\omega)$ becomes coupled with its transverse counterpart, $C_T(Q,\omega)$, which essentially involves velocity components orthogonal to $\hat{\mathbf{Q}}$. This coupling is revealed by a double-peaked structure of both $C_T(Q,\omega)$ and $C_l(Q,\omega)$, and thus of $S(Q,\omega)$, through Eq. 1. In water, such double-peaked structure was actually evidenced by several IXS determination of $S(Q,\omega)$[7–9], as well as by MD simulations of $C_T(Q,\omega)$, $C_l(Q,\omega)$ and $S(Q,\omega)$[10,11,28].

Within the memory function formalism[27], the choice of the actual model to approximate the spectral shape $S(Q,\omega)$ requires a suited *ansatz* for the time decay of the memory function. This is usually achieved by either assuming that such decay has the form of a simple exponential law (Debye, or viscoelastic, model) or using more realistic, yet complex approximations, involving multiple relaxation timescales, or even continuous distributions of them. The line-shape model we used was successfully employed in several IXS experiments on hydrogen bonded liquids[18,29], noble gases[30], liquid metals[31], diatomic liquids[32], supercooled molecular systems[33] and glasses[34]. Its explicit derivation can be achieved in the framework of the memory function formalism and eventually leads to following form for the

normal0ized dynamic structure factor[27]:

$$S_l(Q,\omega) = \frac{1}{\pi}\frac{\omega_T^2(Q)m'(Q,\omega)}{\left[\omega^2 - \omega_T^2(Q) - \omega m''(Q,\omega)\right]^2 + \left[\omega m'(Q,\omega)\right]^2}, \tag{3}$$

where the suffix "l" in the left hand side stands for "longitudinal", thus indicating that Eq. 3 describes the merely longitudinal part of the spectrum, as predicted simple hydrodynamic theory[27], i.e. the one expected when neglecting any coupling with transverse current fluctuations. The variable $\omega_T = c_T(Q)Q$ represents the isothermal sound dispersion, with $c_T(Q)$ being the finite-Q generalization of the isothermal sound velocity. The functions $m'(Q,\omega)$ and $m''(Q,\omega)$ in Eq. 3 are, respectively, the real and the imaginary parts of the Fourier transform of the second order memory function $m(Q,t)$. The latter can be approximated by the sum of two exponential decay terms[18,27,29,32] plus another term $\propto \delta(t)$ accounting for fast rearrangements of molecular degrees of freedom ("instantaneous relaxation"):

$$m_{VE}(Q,t) = A\delta(t) + \left[\omega_l^2 - \omega_0^2\right] e^{-\frac{t}{\tau}} + \omega_0^2\left[\gamma - 1\right] e^{-\gamma D_T Q^2 t}, \tag{4}$$

where τ, ω_0 and ω_l are the relaxation time, the zero and infinite frequency (viscous and elastic) longitudinal sound dispersions, respectively; D_T and γ are the finite-Q generalizations of thermal diffusivity and specific heat ratio, respectively, while A denotes the strength of the "instantaneous" relaxation process. All of these variables should be considered as Q-dependent even if, for the sake of simplicity, the explicit reference to such dependence is omitted in the notation. The Fourier transform of Eq. 4 yields a complex function whose real and imaginary parts can be inserted into Eq. 3 to finally obtain a line-shape model of the longitudinal part of the spectrum. Consistent to what was proposed in Refs. 8 and 9, the additional peak in the spectrum generated by the L-T coupling is here approximated by a simple Damped Harmonic Oscillator DHO[35] term:

$$\frac{S(Q,\omega)}{S(Q)} = (1-\tilde{T})S_l(Q,\omega) + \tilde{T}\frac{1}{\pi}\frac{2\Omega_t^2\Gamma_t}{\left[\omega^2 - \Omega_t^2\right]^2 + 4\Gamma_t^2\omega^2}, \tag{5}$$

where Ω_t and Γ_t represent, respectively, the characteristic frequency and damping of the low-frequency excitation, while $\tilde{T}$ is a Q-dependent scaling factor yielding the relative weight of the DHO component. Within the hypothesis

that the DHO term arises from the L-T coupling, $\tilde{T}$ provides a measure of the strength of such coupling.

The present choice of approximating the double inelastic feature by the sum of two distinct model functions is merely empirical. A more rigorous model of the spectral shape should be based upon a suitable expression of the memory function able to reproduce the double-excitation feature. Such a formalism should also be extended to a time domain much shorter than the structural relaxation time and to mesoscopic distances. Clearly at these distances symmetry arguments leading to assume a perfect decoupling between transverse and longitudinal velocities no longer apply and a coupling L-T mechanism must be taken into account. Furthermore, in order to be compliant with classical hydrodynamics, the model lineshape should be able to describe the Q-evolution of the transverse mode from a low-Q (non-propagating) quasi-elastic peak towards a high-Q well resolved inelastic excitation. Such a model is not yet available in the literature, however we are currently working toward the achievement of this goal.

A preliminary attempt to model the low frequency peak with a pure viscoelastic function (see, e.g., Ref. 51) in place of the DHO term, provided poor results. This was due to the interference of its quasi-elastic peak with the one of $S_l(Q,\omega)$ (Eq. 3), when fitting the central part of the spectrum. Such crosstalk propagated immediately to the inelastic part of the model, since in a viscoelastic function all spectral parameter are mutually intertwined. Conversely, the use of a DHO function as a model for the low-frequency peak provided more reliable fitting results. This is owing to the following reasons: i) the DHO function contains a reasonably small number of line-shape parameters and ii) it lacks of its own quasi-elastic peak, which minimizes the aforementioned interference effects. Additionally, the DHO has been used in literature to describe the spectrum of systems as diverse as glass formers[36], glasses[37], water[1,2,5–7,38], noble gases[39], quantum[40] and classical crystals[13]. More specifically, a model similar to the one used in this work, i.e. consisting in the sum of a viscoelastic and a DHO function was successfully used to account for L-T coupling effects in the water spectrum[8,9]. Also, the DHO function can be formally derived within the memory function framework by simply assuming $m(Q,t) \propto \delta(t)$ (Markovian approximation), which implies that the relevant relaxation timescales are much shorter than the inverse of the characteristic frequency of the mode. The hypothesis that the transverse component of the spectrum is closely approximated by a simple DHO is likely more sound in the highest probed Q-range, where, indeed, $\tau \ll \Omega_t^{-1}$ and, correspondingly, the low frequency excitation is better resolved.

IV. DATA ANALYSIS

In order to fit the experimental spectra, we have minimized a χ^2 variable defined as the normalized distance between the experimental line shape and the following model profile:

$$I(Q,\omega) = Kf(\omega)S_M(Q,\omega) \otimes R(\omega) + B. \quad (6)$$

Here $f(\omega) = \hbar\omega/k_BT[1 - \exp(-\hbar\omega/k_BT)]$ is the detailed balance factor accounting for the statistical population of states with different frequency, R(ω) is the instrumental resolution function and the symbol "$\otimes$" represents the convolution operator. Finally, K and B are two ω-independent terms representing, respectively, an overall scaling factor and a plateau which in principle includes the spectral background and the electronic noise of the detectors ($<$ 1 mHz). During the fitting routine the latter two parameters, along with an overall shift of the ω-axis, have been left free to vary, with no external constraints.

In order to limit the number of free fit parameters, it is useful to superimpose the compliance of the model with sum rules, which allows to fix some of them. Specifically, the fulfilment of the two lowest-order sum rules leads to the following expression for the 0-frequency limiting dispersion[27]:

$$\omega_0 = \sqrt{\frac{\gamma K_B T}{MS(Q)}}Q = c_s Q\sqrt{\frac{S(0)}{S(Q)}} \quad (7)$$

where K_B, M, c_s and $S(Q)$ are the Boltzmann constant, the molecular mass, the adiabatic sound velocity and the static structure factor, respectively. Consistent with what has been suggested by similar studies in literature[8,18,41], in the second part of Eq. 7 we have assumed $\gamma(Q) \approx \gamma$ where γ is the macroscopic limit ($Q \to 0$) of the corresponding Q-dependent variable. Also consistent with previous literature (see Refs. 8 and 18), in Eq. 4 we decided to neglect the term $\propto (\gamma - 1)$, since for water $\gamma \approx 1$[42] in the probed T-range . Furthermore, the knowledge of c_s and $S(Q)$, provided by a NIST[42] and a neutron scattering[43] databases respectively , allows us to fix ω_0, thus removing a fitting parameter.

The strategy adopted to best fit liquid phase spectra is based on the iterative procedure schematized in the following:

i) Preliminary best fit of IXS spectra: in this first step all line-shape parameters have been left free to vary, apart from Ω_0, which was determined through Eq. 7. Overall, we observed a large statistical correlation between the parameters describing the low-frequency excitation (T, Ω_t and Γ_t) and the one essentially defining the width of the quasi-elastic peak, i.e. the relaxation time, τ. Ultimately, such a strong correlation was due to the relatively coarse

IXS resolution, which prevented a reliable determination of the spectral shape in the quasi-elastic region. Conversely, a negligible statistical correlation affected the determination of shape parameters entering in the high-frequency (longitudinal) mode, i.e. ω_l and A.

ii) Successive best fit of INS spectra: here ω_l and A were fixed to the values optimized in the previous fitting routine, while ω_0 was again kept fixed to the value predicted by Eq. 7. Thanks to the narrower resolution and higher spectral contrast, best fits of INS data delivered more reliable results. In particular, optimized values of T, Ω_t, Γ_t and τ appeared rather less correlated than when fitting IXS spectra. Also, the rather narrow frequency domain spanned by INS made the fitting results only marginally sensitive to the specific values of the fix parameters ω_l and A, which are mostly related with the longitudinal mode.

iii) Further best fit of IXS spectra: in this last step only ω_l and A were left free to vary, while best fit results of INS spectra were used to fix the other parameters.

Above we only described the first three core steps of the iterative procedure, both for the sake of simplicity and because they were often sufficient to reach the final optimization; however, in few cases, additional iteration steps were needed.

When fitting INS spectra of solid D_2O, we used model line-shape consisting in a double DHO profile accounting for the side (transverse and longitudinal) peaks plus a $\delta(\omega)$ function describing the elastic scattering. As discussed above, the choice of the DHO functions is somehow arbitrary. However, in the case of solid D_2O, the use of alternative peak functions, as Lorentzian or Pseudo-Voigt profiles provided essentially identical results.

V. DISCUSSION

Typical INS line-shapes are compared in Fig. 1 with corresponding IXS ones. Negative values of $\hbar\omega = E_i - E_f$ refer to the energy gain side of the neutron/x-ray spectrum, E_f being the neutron/x-ray energy after the scattering event. The spectra shown in Fig. 1 were obtained after background subtraction and normalization to the integrated intensity. The latter was estimated by numerical evaluation of the integral $\int_{-\omega_M}^{\omega_M} I(Q,\omega)d\omega$, where $I(Q,\omega)$ is the best fit value of Eq. 6 as obtained evaluating the model function $S_M(Q,\omega)$ over the $\pm\omega_M$ ($\pm$ 400 THz) frequency range.

These spectra provide thus a reliable measure of the normalized dynamic structure factor $S_n(Q,\omega) = I(Q,\omega)/I(Q)$. Each $S_n(Q,\omega)$ spectrum is reported alongside the corresponding longitudinal current spectra, $(\omega/Q)^2 S_n(Q,\omega)$. Both IXS and INS energy resolution functions are reported in the bottom left panel for comparison. When comparing INS and IXS line-shapes in Fig. 1, one readily notices the quite sharper profile of INS spectra, due to the Gaussian shape of the resolution , which allows them to reproduce in great detail the low frequency features of the true sample spectrum. This appears even more clear as one looks at the current spectra. In fact the shape of the low frequency mode can be clearly discerned in the INS profiles, while in IXS ones it is hidden by the large resolution tails at least for $Q \leq 12$ nm^{-1}. However, the high frequency longitudinal mode lies definitely out of the INS domain, while it is well inside the one of IXS.

Upon increasing Q, one may also notice that: i) for $Q \leq 12nm^{-1}$, the longitudinal mode broadens and its position (down arrow) correspondingly shifts to higher frequencies; conversely, the low frequency peak exhibits a relatively weaker Q-dispersion. In the $Q = 16\ nm^{-1}$ spectrum the longitudinal peak seemingly reverses its Q-trend, shifting back towards the elastic ($\omega = 0$) position. This seems consistent with the expected $\propto Q/S(Q)$ trend of the dispersion; ii) the intensity of the low-frequency mode undergoes a systematic Q-increase, consistent with the expected enhancement of the L-T coupling; iii) eventually, at 16 nm^{-1}, the two peaks have comparable intensity and can barely be resolved from each other. In the plot, the smoothed profile is reported as a guide-to-eye to emphasize the presence of a double-peaked structure. Overall, the plotted data are qualitatively similar to longitudinal current profiles simulated by MD techniques at overlapping Q values, yet in different thermodynamic conditions (see Fig. 1c of Ref. 11).

In Fig. 2 corrected INS spectra are reported against their best fit line-shape, along with the DHO component accounting for the low-frequency mode. We notice that the inelastic shoulder undergoes a gradual evolution from an intermediate-Q, viscoelastic, regime where it is clearly over-damped, to a high-Q one where it assumes the form of an under-damped inelastic excitation. This trend is certainly interesting and worth further comment. As demonstrated in Ref. 18, a viscoelastic analysis of IXS spectra of water can be carried out at relatively small Q's with no need of additional low-frequency inelastic modes. In such "viscoelastic" regime the spectrum can be modeled assuming ω-dependent transport parameters, which, upon increasing ω, gradually evolve from the viscous to the elastic limit[44]. This trend reveals the presence of an active relaxation process, whose most visible effects on the spectral shape are:

i) the rise of an additional quasi-elastic feature having a $\propto 1/\tau$ width, customarily referred to as the "Mountain peak"[45] and ii) the shift of the longitudinal acoustic frequency from $\Omega_0(Q)$ to $\Omega_l(Q)$ (positive sound dispersion). The viscoelastic phenomenology of the water spectrum has been extensively studied by IXS[18,46–48] and INS[3,4], as well as by complementary techniques such as, e.g., Brillouin visible Light[49], or UV[50] Scattering. Indeed, in the lowest Q INS spectra of Fig. 2, the two low-frequency side-peaks merge transforming in a single over-damped, quasi-elastic feature, nearly isomorph to the Mountain peak and thus hardly distinguishable from it. Therefore the viscoelastic function is likely to provide an accurate approximation of the line-shape at low Q's ($Q \leq 6\ nm^{-1}$), where the Mountain peak and the over-damped transverse mode have essentially the same shape. For IXS spectra this difficulty is certainly worsened by the relatively coarse energy resolution function, which also explains why in some IXS studies the low frequency feature could not be detected. Due to either the low Q[18] or high T[47] probed in these works, the low frequency peak could hardly emerge from the broad and intense resolution wings.

Such behavior is illustrated more quantitatively by Fig. 3, where the Q-dependence of Ω_t is reported along with the ones of Γ_t, $1/\tau$ and Ω_l^{IXS}. The latter variable is defined as the position of the high frequency peak of IXS current spectra (see down arrows in Fig. 1), which provides a realistic and essentially model-free estimation of the longitudinal frequency. The determination of Ω_l^{IXS} allows us to perform a reliable comparison with the longitudinal frequency measured in Ref. 8. However, in such work the latter was determined using the viscoelastic part of best-fit $S(Q,\omega)$, rather than considering the whole, experimentally measured, line-shape. If, from one side, the obtained values of Ω_l^{IXS} is model-free, from the other, it can be slightly affected by the convolution with the finite resolution function. We recall that the longitudinal frequency is the natural outcome of MD simulations and this give us a matter for a more general comparison with literature results, as discussed farther below (see Fig. 4).

Before comparing IXS and INS results, one should consider the so called kinematic limitations affecting neutron scattering. We recall that the boundary of the dynamic region accessible by INS can be determined from the energy and momentum conservation laws of the scattering event[51], the resulting curve is reported in Fig. 3 for comparison. One readily notices that the longitudinal peak falls out of the INS domain at all Q's, while it is well inside the dynamic range spanned by IXS spectral tails.

At high Q's the $1/\tau$ data largely exceed the maximum frequencies covered by INS thus making the determination of this parameter gradually less reliable. These values are not included the plots of Fig. 3 being out of the scale. It can be noticed that, for $Q \to 0$, Ω_l^{IXS}, tends to zero, while $1/\tau$ must tend to a finite value (determined by the

Maxwell relaxation time). Consequently, at some momentum transfer lying below the probed Q-range, the condition $\Omega_l^{IXS} \approx 1/\tau$ must be met. This marks the viscoelastic crossover, i.e. the transition from the merely viscous (liquid-like) behavior to the elastic (solid-like) one. Therefore the curves demonstrate that the viscoelastic crossover occurs below the lowest boundary of the probed Q range. Once the transition to the elastic regime is fully accomplished, the onset a transverse mode in the spectrum becomes allowed. For $Q > 12\ nm^{-1}$, the IXS current spectra no longer exhibit a single clear maximum, they rather assumes a more complex double-peaked shape due to the large strength of the L-T coupling. At these Q's, Ω_l^{IXS} was determined after smoothing by interpolation the $(\omega/Q)^2 S(Q,\omega)/S(Q)$ profiles (see, e.g., the top-right panel of Fig. 1), which made easier the determination of Ω_l^{IXS}.

In this region the low-frequency mode has a strongly over-damped character and, consequently, Ω_t cannot be realistically interpreted as a propagating frequency and it should, instead, be considered as a characteristic, or dominant, frequency of the current spectrum (see Fig. 1). When moving towards higher Q's, the shear mode assumes the form of an under-damped inelastic peak ($\Gamma_t < \Omega_t$) . The crossover between a non-propagating and a propagating nature can be described assuming that the corresponding eigenvalue of the hydrodynamic matrix, $\propto \eta_s(Q)$, acquires a non-vanishing imaginary part at high Q's. Plotted data demonstrate that in over-damping region also $\Gamma_t \approx 1/\tau$, while the difference between the two parameters systematically increases upon increasing Q. This might suggest that at low-Q the physical process hampering the propagation of shear waves is its interaction with the structural relaxation. In Fig. 4 we compare dispersion curves of water reported in literature with the values of Ω_t, Ω_l^{IXS} and Ω_t^{INS} obtained in this work. The latter variable represents the positions of the low frequency peaks in current spectra as evaluated from INS measurements. Since all dispersions measured in this work were found to be fairly insensitive to T changes, they are reported after T-averaging. Again, the error bars represent the standard deviations of such a T-average and, for Ω_t^{INS}, they are well within the symbols size. When comparing our measurements to each other, it clearly emerges than Ω_t^{INS} values are systematically higher than Ω_t ones. We recall that the former were derived from the current spectra evaluated using experimental INS line-shapes, while the latter are obtained from best fit parameter of the model function. Certainly, Ω_t^{INS} provides a more reliable determination of the low frequency dispersion since it is intrinsically model-free and it has been determined from the whole spectral shape rather than from its DHO component only.

An examination of the low frequency dispersions in Fig. 4 reveals a discrepancy between Ω_t^{INS} and literature dispersion curves at the lowest Q's ($Q \leq 10 nm^{-1}$). This can be partly explained considering the observed over-damped character of shear modes within such a Q-range. Another factor challenging previous literature results is the low

Q dispersion of the transverse peak. Below $\approx 10\ nm^{-1}$ the Q increase of Ω_t^{INS} seems consistent with a Q^2-law, while for a propagating acoustic mode it is expected to be linear. This finding further questions the propagating nature of the shear mode in the low Q-range. Discrepancies between present data and literature results can be ascribed, in some cases, to the different shape of the resolution function. Another relevant factor may be the different thermodynamic state of the sample. In fact, in previous IXS works, the low-frequency (under-damped) excitation was observed only at lower temperatures (close or below the melting) and/or at higher pressures[7–9], while here it is probed at ambient pressure and at temperatures $\geq$ 285 K. Such different thermodynamic conditions may affect the propagating character of the low frequency mode. In this respect, it's worth mentioning the neutron scattering work of Bermejo et al.[2], performed in a thermodynamic state close to the ones of the present experiment and suggesting the presence of a largely damped mode at frequencies close to Ω_t^{INS} (see Fig. 4). Most important, present data are obtained with unprecedented energy resolution and spectral contrast, which certainly makes them more trustworthy than previous measurements.

On the right hand plot of Fig. 4 we also report for comparison the Density of States (DoS) measured by Incoherent Neutron Scattering[52]. The comparison with this profile suggests that the peak at 6 meV is related to the weakly dispersing low-energy mode, extensively discussed in this work and customarily ascribed to a propagating shear wave.

The T-dependence of τ is plotted in Fig. 5 as measured at various Q's. The values are derived from the aforementioned iterative analysis and are compared with the one resulting from the preliminary fitting of the IXS spectra, in which all parameter were left free to vary without any constraints; the latter data extend at Q's below 6 nm^{-1} where INS spectra are not available. Experimental curves are also compared with their Q=0 counterpart as extracted from ultrasound absorption measurements reported in Ref. 53, as well as with the shear viscosity[42] re-scaled by an arbitrary factor. Noticeably, experimental data exhibit the expected systematic decrease with Q, but even at the lowest Q's they still fall far below their macroscopic ($Q = 0$) limit. Moreover, one can observe that, at any Q, the reported data follow the same T-decrease, which parallels the one of shear viscosity. This behavior reveals the structural nature of the active relaxation process, consistent with previous IXS results obtained in simple[30] and associated[18,47] liquids, as well as in supercritical systems[41].

In Fig. 6 the limiting dispersions ω_0 and ω_l are reported along with $1/\tau$ and Ω_l^{IXS}. At low and intermediate Q's, Ω_l^{IXS} is systematically higher than ω_0 and almost identical to ω_l. This trend confirms what was already observed in Fig.3, i.e. that the crossover of Ω_l^{IXS} from the viscous (ω_0) to the elastic (ω_l) regimes, is already accomplished even

at the lowest Q's (and lowest T's) probed in this experiment. However, owing to both the sharp Q-increase of $1/\tau$ and the bending of Ω_l^{IXS} the viscoelastic condition, $\Omega_l^{IXS}\tau \approx 1$ is met also at higher Q values falling in the range probed by the present experiment. This roughly happens when the line-plus-symbols curves in Fig. 3 (representing Ω_l^{IXS} and $1/\tau$) cross each other. Upon further increasing Q, one should expect a back transition of Ω_l^{IXS} from the elastic (ω_l) to the viscous value (ω_0), as previously observed in literature (see e.g. Fig. 4 of Ref. 32). Interestingly enough, in the present experiment Ω_l^{IXS} does not rejoin ω_0, rather remaining close to ω_l. This suggests that the elastic regime extends in water over a larger high-Q range, probably due the presence of the L-T coupling. One may notice that, at some T's, Ω_l^{IXS} values exceed their elastic limit ω_l, which is clearly inconsistent with physical expectations. This result probably reveals the inadequacy of the adopted model to describe the highest Q spectra. In fact Ω_l^{IXS} values are model-free, while ω_l's are not and they are probably underestimated at high Q. The overall scenario depicted by Fig. 6 confirms what was already found in Ref. 8 and leads us to conclude that the shear mode shows up in the $S(Q,\omega)$ when the system joins its elastic regime; here, indeed, the L-T coupling is expected to be more effective.

The Q-dependence of τ at T =295 K is reported in Fig. 7 as determined either by the full iterative fitting procedure of INS spectra or from the unconstrained fit of IXS ones. The logarithmic plot emphasizes the rapid, nearly exponential, Q-decay, almost parallel for INS and IXS data; however, the absolute values determined from IXS spectra are slightly higher. Aside from the weak distortion induced on the fitting results by MS effects, as discussed in the experimental section, other possible sources of such discrepancy are inherent to the line-shape modeling.

In fact, when performing the totally unconstrained best fitting of IXS spectra, we observed that the latter systematically delivered a vanishing intensity for the DHO term in Eq. 5 at least for $Q \leq 14nm^{-1}$. This trend was accompanied by a parallel overestimation of both intensity and width of the quasi-elastic relaxational mode, the aforementioned Mountain peak. The link between these two trends is straightforward since the Mountain peak has a width $\propto 1/\tau$, therefore an overestimation of its width corresponds to an underestimation of the relaxation time. The competition between the intensities of transverse and relaxational modes is fostered by the largely damped nature of the former, which makes the two modes hardly distinguishable from each other at low Q's, or, as shown in Ref. 8, at low densities. Such a strong interplay makes difficult the proper detection of the shear mode; such problem is clearly worsened by the relatively low spectral contrast provided by the IXS resolution shape.

Further information on the phenomenological aspects of the L-T coupling can be gained from the comparison between the dynamic behavior of the liquid and the solid phases, as discussed further below.

Under moderate pressures and temperatures water freezes in the ice hexagonal (Ih) structure, characterized by a nearly perfect tetrahedral network of hydrogen bonds. There are six possible orientations for a water molecule in its tetrahedral bonding environment, each corresponding to a different arrangement of protons in the four H-bonds. In ice Ih all possible orientations of the water molecule at each lattice site are equally represented. Therefore we can describe the structure of ice as an ordered hexagonal lattice for the oxygen atoms and a random distribution of the deuterium atoms in one of the two available sites between two neighboring oxygens. The phonon dispersion relations in Ih have been studied by IXS,[13] INS[54–57] and MD simulations[55,56] both in poly- and single-crystals. Generally, it has been found that the phonon frequencies of both longitudinal and transverse branches were essentially unchanged in the two structures.

The Q-evolution of INS spectra in the solid phase is illustrated in Fig. 8, where they are reported against the corresponding best fit line-shapes and the two DHO components separately accounting either for the transverse or for the longitudinal mode. We observed the presence of two well-resolved peaks. One of them is centered at around 6 meV and it is usually ascribed to an Optic Transverse (OT) mode[13]. We recall here that the OT nature of the mode has been suggested by Ref. 13, in agreement with previous works on ice[54], based on: i) the absence of a clear Q-dispersion and ii) the disappearance of this mode at Q's below the reduced zone boundary (7.5 nm^{-1}). In the right panel of Fig. 9 we report for comparison the INS measurement of DoS performed by by Davidowski et al.[57]. In analogy with the results achieved in the liquid phase (see Fig. 4, right panel), we believe that the peak at 6 meV has to be related to such weakly dispersing OT mode. The comparison between the dispersions in liquid and solid phases suggests that such OT-mode is actually the solid-phase counterpart of the transverse mode we observe in the liquid. The spectra also show the presence of a second, sharp peak, which is particularly intense at 16 nm^{-1}. This is the longitudinal acoustic mode, which is characterized by a very steep Q-dependence, also appreciable by comparing the bottom (Q= 16 nm^{-1}) and upper panels (Q= 24 nm^{-1}). This brings its characteristic frequency into a deep minimum around the boundary of the second pseudo Brillouin zone (i.e., at $Q \approx 15\ nm^{-1}$), owing to the destructive interference between the acoustic wave and the crystal periodicity. The position of such longitudinal mode appear consistent with the measurement of the longitudinal branch in ice performed by Criado et al.[55] and reported for comparison in Fig. 9.

The best fitting procedure of ice spectra allowed us to extract fairly T-independent values for both the characteristic frequency (Ω_t) and damping (Γ_t) of the OT mode. The optimized values of these two parameters are reported in Fig. 9 after T-average and as a function of Q, along with the corresponding quantities determined in the liquid phase (T=295 K). We recognize that Ω_t undergoes a neat increase at the crossover from the liquid to the solid phase. Such discontinuity reduces with increasing Q. Conversely, the Γ_t value seems quite less sensitive to the aggregation phase. This behavior is consistent with the results reported in Ref. 58, where it is shown that the phonon line-width in Ih is largely determined by anharmonicity effects rather than the structural disorder. The present data suggest that the order-disorder transition of the structure consequent to the melting does not dramatically affect the parameter Γ_t.

VI. CONCLUSION

In summary, we presented the first experimental characterization of the THz spectrum of water by the combined use of two complementary spectroscopic techniques, Inelastic X-ray and Neutron Scattering (IXS and INS respectively). The combination of these techniques allowed us, on one hand, to probe the $S(Q,\omega)$ of water with unprecedented narrow (0.1 meV, FWHM) and sharp (nearly Gaussian) resolution function and, on the other hand, to take advantage of the parallel use of IXS, a technique virtually free from kinematic limitations, thus dramatically extending the frequency range probed by INS. As a result, we observed that a clear two-peak structure characterizes the dynamic response of water at relatively high wave-vectors. The additional, low-frequency and weakly-dispersive mode was already observed in the literature and associated with the onset of a longitudinal-transverse coupling. We demonstrate that such additional peak undergoes a crossover from a low-Q regime, in which it is clearly over-damped, towards a higher Q regime, where it assumes the form of a inelastic peak clearly resolved in the spectrum. Moreover in the over-damping region the dominant frequency of the transverse mode turns out to be comparable with the inverse of the structural relaxation time, suggesting that in this dynamic window the interaction of the structural relaxation hampers the propagation of well-defined shear waves. The relaxation time-scales measured by the two techniques exhibit similar Q and T-dependencies, revealing the structural nature of the observed relaxation process. When the sample reaches its solid phase an important increase of the transverse peak frequency is observed, while its line-width is substantially unaffected. This finding endorses the picture that the phonon lifetime in hexagonal ice is essentially related to anharmonic interactions rather than to structural disorder. Most important, the differences related to the aggregation phase of water tends to disappear at high wave-vectors. The latter finding further emphasizes the

solid-like nature of the water dynamics when probed over small distances.

Acknowledgments

The authors feel deeply indebted to Dr U. Bafile and Dr E. Guarini both for their valuable help in setting up the fitting program and for providing to us the computation of double scattering intensity effects. Moreover they acknowledge the technical and scientific support from both SNS and APS staff. A. C. and C. N. K. acknowledge NSLS-II project for funding the travel to SNS. Research at Oak Ridge National Laboratory's Spallation Neutron Source was supported by the Scientific User Facilities Division, Office of Basic Energy Sciences, U. S. Department of Energy. The use of the Advanced Photon Source at Argonne National Laboratory was supported by the U. S. Department of Energy, Office of Science, Office of Basic Energy Sciences, under Contract No. DE-AC02-06CH11357. The construction of HERIX was partially supported by the NSF under Grant No. DMR-0115852. Dr T. Rowell is acknowledged for the critical revision of the manuscript.

[1] 6.P. Bosi, F. Dupre, F. Menzinger, F. Sacchetti, and M. C. Spinelli, Lett. Nuovo Cimento Soc. Ital. Fis. **21**, 436 (1978).

[2] F. J. Bermejo, M. Alvarez, S. M. Bennington, and R. Vallauri, Phys. Rev. E **51**, 2250 (1995).

[3] C. Petrillo , F. Sacchetti , B. Dorner , J.B. Suck, Phys.Rev. E **62**, 3611 (2000);

[4] F. Sacchetti, J.-B. Suck, C. Petrillo, and B. Dorner, Phys. Rev. E **69**, 061203 (2004).

[5] F. Sette, G. Ruocco, M. Krisch, U. Bergmann, C. Masciovecchio, V. Mazzacurati, G. Signorelli, and R. Verbeni, Phys. Rev. Lett. **75**, 850 (1995).

[6] G. Ruocco, F. Sette, U. Bergmann, M. Krisch, C. Masciovecchio, V. Mazzacurati, G. Signorelli, and R. Verbeni, Nature (London) **379**, 521 (1996).

[7] F. Sette, G. Ruocco, M. Krisch, C. Masciovecchio, R. Verbeni, and U. Bergmann, Phys. Rev. Lett. **77**, 83 (1996).

[8] E. Pontecorvo, M. Krisch, A. Cunsolo, G. Monaco, A. Mermet, R. Verbeni, F. Sette, and G. Ruocco, Phys.Rev. E **71**, 011501 (2005).

[9] A. Cimatoribus, S. Saccani, F. Bencivenga, A. Gessini, M.G. Izzo, C. Masciovecchio, New J. Phys. **12**, 053008 (2010).

[10] A. Rahman and F.H. Stillinger Phys. Rev. A **10**, 368 (1974).

[11] M. Sampoli , G. Ruocco , F. Sette Phys. Rev. Lett. **79**, 1678 (1997).

[12] An alternative account for the double-mode structure of the water spectrum is proposed in Refs. 3 and 4. It stems from the idea that the acoustic and a high frequency optic-like mode repel each other in order to avoid crossing. Although this interpretation explains the basic phenomenology, it is inherently unable to link the rise of the low-frequency mode to the structural relaxation nor to explain the observed T-dependence[8].

[13] G. Ruocco, F. Sette, M. Krisch, U. Bergmann, C. Masciovecchio and R. Verbeni, Phys. Rev. B **54**, 14892 (1996).

[14] T. Scopigno, E. Pontecorvo, R. Di Leonardo, M. Krisch, G. Monaco, G. Ruocco, B. Ruzicka, F. Sette, J.Phys. Condens. Matter **15**, S1269 (2003).

[15] R. Dell'Anna, G. Ruocco, M. Sampoli and G. Viliani, Phys. Rev. Lett. **80**, 1236 (1998);B. Ruzicka, T. Scopigno, S. Caponi, A. Fontana, O. Pilla, P. Giura, G. Monaco, E. Pontecorvo, G. Ruocco and F. Sette, Phys. Rev. B **69**, 100201 (2004).

[16] L. E. Bove, E. Fabiani, A. Fontana, F. Paoletti, C. Petrillo, O. Pilla and I. C. V. Bento, Europhys. Lett. **71**, 563 (2005).

[17] L. Orsingher, G. Baldi, A. Fontana, L. E. Bove, T. Unruh,A. Orecchini, C. Petrillo, N. Violini and F. Sacchetti, Phys. Rev. B **82**, 115201 (2010).

[18] G. Monaco, A. Cunsolo, G. Ruocco, and F. Sette, Phys. Rev. E **60**, 5505 (1999).

[19] G. Ehlers, A. A. Podlesnyak, J. L. Niedziela, E. B. Iverson and P. E. Sokol, *Rev. Sci. Instrum.* **82**, 085108 (2011)

[20] C. F. Koehler and J. Z. Larese,Rev. Sci. Instrum. **71**, 324 (2000).

[21] For further details on see the website: http://www.aps.anl.gov/Beamlines/Directory/

[22] T. S. Toellner, A. Altas and A. H. Said, J. Synchrotron Rad. **18**, 605 (2011); A. H. Said, H. Sinn, and R. Divan, J. Synchrotron Rad. **18**, 492 (2011).

[23] V.F. Sears, Can. J. Phys. **44**, 1299 (1966); ibid. **45**, 237 (1966).

[24] J. Teixeira, M.C. Bellissent-Funel, S.H. Chen and A.J. Dianoux, Phys. Rev. A **31**, 1913 (1985).

[25] E. Guarini and U. Bafile, private communication.

[26] They simulated the single and double scattering intensity assuming that a $E_i = 20$ meV energy incident beam is impinging at normal incidence on a 0.5 mm D_2O slab. We stress that for a thin sample, double scattering effects provide the leading contribution to the total MS.

[27] U. Balucani and M. Zoppi, "Dynamics of the Liquid State" (Clarendon Press, Oxford, 1994).

[28] U. Balucani, J. P. Brodholt and R. Vallauri, J. Phys. Condens. Matter **8**, 9269 (1996)

[29] R. Angelini, P. Giura, G. Monaco, G. Ruocco, F. Sette and R. Verbeni, Phys. Rev. Lett. **88**, 255503 (2002).

[30] A. Cunsolo, G. Pratesi, G. Ruocco, M. Sampoli, F. Sette, R. Verbeni, F. Barocchi, M. Krisch, C. Masciovecchio and M. Nardone, Phys. Rev. Lett. **80**, 3515 (1998).

[31] T. Scopigno, G. Ruocco and F. Sette, Rev. Mod. Phys. **77**, 881 (2005).

[32] F. Bencivenga, A. Cunsolo, M. Krisch, G. Monaco, G. Ruocco and F. Sette, Europhys. Lett. **75**, 70 (2006).

[33] L. Comez, D. Fioretto, G. Monaco, G. Ruocco, J. Non-Crys. Solids **307-310**, 148 (2002); F. Scarponi, L. Comez, D. Fioretto and L. Palmieri, Phys. Rev. **B 70**, 054203 (2004).

[34] G. Ruocco, F. Sette, R. Di Leonardo, G. Monaco, M. Sampoli, T. Scopigno and G. Viliani, Phys. Rev. Lett. **84**, 5788 (2000).

[35] U. Bafile, E. Guarini and F. Barocchi, Phys. Rev. E **73**, 061203 (2006).

[36] G. Monaco, C. Masciovecchio, G. Ruocco and F. Sette, Phys. Rev. Lett. **80**, 2161 (1998);G. Ruocco, F. Sette, R. Di Leonardo, D. Fioretto, M. Krisch, M. Lorenzen, C. Masciovecchio, G. Monaco, F. Pignon and T. Scopigno, Phys. Rev. Lett. **83**, 5583 (1999);D. Fioretto, U. Buchenau, L. Comez, A. Sokolov, C. Masciovecchio, A. Mermet, G. Ruocco, F. Sette, L. Willner, B. Frick, D. Richter and L. Verdini Phys. Rev. E **59**, 4470 (1999); O. Pilla, A. Cunsolo, A. Fontana, C. Masciovecchio, G. Monaco, M. Montagna, G. Ruocco, T. Scopigno and F. Sette, Phys. Rev. Lett. **85**, 2136 (2000).

[37] C. Masciovecchio, G. Ruocco, F. Sette, M. Krisch, R. Verbeni, U. Bergmann and M. Soltwisch, Phys. Rev. Lett. **76**, 3356 (1996); P. Benassi, M. Krisch, C. Masciovecchio, V. Mazzacurati, G. Monaco, G. Ruocco, F. Sette and R. Verbeni, Phys. Rev. Lett. **77**, 38353838 (1996); C. Masciovecchio, G. Ruocco, F. Sette, P. Benassi, A. Cunsolo, M. Krisch, V. Mazzacurati, A. Mermet, G. Monaco and R. Verbeni, Phys. Rev. B **55**, 8049(1997).

[38] A. Cunsolo, G. Ruocco, F. Sette, C. Masciovecchio, A. Mermet, G. Monaco, M. Sampoli and R. Verbeni, Phys. Rev. Lett. **82**, 775 (1999).

[39] A. Cunsolo, G. Pratesi, R. Verbeni, D. Colognesi, C. Masciovecchio, G. Monaco, G. Ruocco and F. Sette, J. Chem. Phys. **114**, 2259 (2001).

[40] C. Seyfert, R. O. Simmons, H. Sinn, D. A. Arms, E. Burkel: J. Phys.: Condens. Matter **11**, 3501 (1999).

[41] F. Bencivenga, A. Cunsolo, M. Krisch, G. Monaco, G. Ruocco and F. Sette, J. Chem. Phys. **130**, 064501 (2009).

[42] http://webbook.nist.gov/chemistry/

[43] http://www.isis.rl.ac.uk/disordered/Database/DBMain.htm

[44] S. W. Lovesey, J. Phys. C: Solid State Phys. **6**, 1856 (1973).

[45] R. D. Mountain, Rev. Mod. Phys. **38**, 205 (1966).

[46] A. Cunsolo, G. Ruocco, F. Sette, C. Masciovecchio, A. Mermet, G. Monaco, M. Sampoli and R. Verbeni, Phys. Rev. Lett. **82**, 775 (1999).

[47] F. Bencivenga , A. Cunsolo , M. Krisch, G. Monaco, G. Ruocco and F. Sette, Phys. Rev. E **75**, 051202 (2007).

[48] F. Sette, G. Ruocco, M. Krisch, C. Masciovecchio, and R. Verbeni, Phys. Scr. **T66**, 48 (1996).

[49] G. Maisano, P. Migliardo, F. Aliotta, C. Vasi, F. Wanderlingh and G. D'Arrigo, Phys. Rev. Lett. **52**, 1025 (1984); G. Maisano, D. Majolino, F. Mallamace, P. Migliardo, F. Aliotta, C. Vasi, and F. Wanderlingh, Mol. Phys. **57**, 1083 (1986); S. Magazù, G. Maisano, D. Majolino, F. Mallamace, P. Migliardo, F. Aliotta and C. Vasi, J. Phys. Chem. **93**, 942 (1989); A. Cunsolo and M. Nardone, J. Chem. Phys. **105**, 3911 (1996).

[50] C. Masciovecchio, S. C. Santucci, A. Gessini, S. Di Fonzo, G. Ruocco and F. Sette, Phys. Rev. Lett. **92**, 255507 (2004); F. Bencivenga, A. Cimatoribus, A. Gessini, M. G. Izzo and C. Masciovecchio, J. Chem. Phys. **131**, 144502 (2009).

[51] S. W. Lovesey, Theory of Neutron Scattering from Condensed Matter, Oxford University Press (Oxford, UK, 1988).

[52] M.-C. Bellissent-Funel, S. H. Chen and J.-M. Zanotti, Phys. Rev. E **51**, 4558 (1995).

[53] K.W. M. Slie , A. R. Donfor and T. A. Litovitz, J. Chem. Phys. **44**, 3712 (1966).

[54] B. Renker, Phys. Lett. A **30**, 493 (1969).

[55] Criado, F.J. Bermejo, M. Garca Hernndez and J.L. Martnez, Phys. Rev. E **47**, 3516 (1993).

[56] F.J. Bermejo, E. Frikee, M. Garca Hernandez, J.L. Martnez and A. Criado, Phys. Rev. E **48**, 2300 (1993)

[57] J. Dawidowski , F. J. Bermejo , C. Cabrillo and S. M. Bennington, Chem. Phys. **258**, 247 (2000).

[58] P. Johansson, Phys. Rev. B **54**, 2988 (1996).

FIGURE CAPTIONS

Fig.1: In the left side of each panels selected $S(Q,\omega)/S(Q)$ line-shapes are reported as measured by IXS ($\bullet$) and INS ($\circ$) spectra after background subtraction and normalization. In the left-bottom panel we also report the energy resolution functions of IXS and INS experiments (full and dotted lines, respectively). The corresponding current spectra $(\omega/Q)^2 S(Q,\omega)/S(Q)$ are shown in the right side of each panel. The black solid line and the thick grey one indicate the IXS and INS profiles respectively, while vertical arrows show the characteristic energy of low and high

frequency excitations of IXS curve. Data were collected at $T = 293\ K$ (INS spectra) and $T = 295\ K$ (IXS spectra) and at the indicated Q-values. In the $Q = 16\ nm^{-1}$ the black line across the curve is obtained as a polynomial interpolation and is intended as a guide-to-the eye.

Fig.2: Some selected INS spectra ($\circ$) are reported with the corresponding best fit line-shape (solid grey line) along with the DHO function (solid black line) accounting for the low frequency transverse mode (see Eq. 5). Data were collected at $T = 293\ K$ and at the Q-values indicated in the individual panels.

Fig.3: The Q-dependence of best fit parameters Γ_t ($\square$) and Ω_t ($\bullet$), are reported along with the ones of $1/\tau$ ($-\star-$) and the longitudinal frequency, Ω_l^{IXS}, extracted from spectral current maxima ($-\blacktriangle-$).

Fig.4: The left panel compares the dispersion curves of water (H_2O and D_2O) as determined by: i) INS measurements (Ref. 1 ($\square$), Ref. 2 ($\triangledown$) and Refs. 3 and 4 ($\lozenge$)); ii) IXS measurements (Ref. 8] ($\times$) and Refs. 5, 6 and 7 ($\bigstar$); iii) MD simulations (Ref. 10 ($\boxtimes$) and Ref. 11 (lines)) compared with the findings of the present work: Ω_t ($\bullet$), the peak position of current spectra (see text) Ω_t^{INS} ($\blacklozenge$) and Ω_l^{IXS} ($-\blacktriangle-$). All measured in this work are averaged over the temperature. The right plot displays the Density of States of water as measured by Incoherent Neutron Scattering (Ref. 52,$\circ$).

Fig.5: Temperature dependence of τ at $Q = 20\ nm^{-1}(-\blacksquare-)$, $Q = 18\ nm^{-1}(-\square-)$, $Q = 16\ nm^{-1}(-\bullet-)$, $Q = 14\ nm^{-1}(-\circ-)$,$Q = 12\ nm^{-1}(-\blacklozenge-)$, $Q = 10\ nm^{-1}(-\lozenge-)$ and $Q = 8\ nm^{-1}(-\blacktriangle-)$. These curves are compared with those derived from the unconstrained best fit of IXS spectra (see text) measured at three lowest Q's: $Q = 2\ nm^{-1}$ ($-\star-$), $Q = 4\ nm^{-1}$ ($-\triangle-$) and $Q = 6\ nm^{-1}$ ($-\nabla-$). The τ values derived from US measurements[53] (dotted line) and the arbitrarily re-scaled shear viscosity[42] are also reported for comparison (dash-dotted line).

Fig.6: Best fit values of parameters ω_l ($\lozenge$), Ω_l^{IXS} ($-\blacktriangle-$) and 1τ ($-\star-$) are reported along with ω_0 ($\circ$), as calculated through Eq. 7, and the low-Q hydrodynamic linear dispersion (dashed lines), as derived from sound velocity data[42].

Fig.7: The Q-dependence of τ at T=295 K, as obtained from the totally unconstrained best fit of IXS data ($\circ$)

and from the iterative fitting routine of both IXS and INS spectra (•).

Fig.8: Representative INS spectra of solid D_2O (T = 268 K), collected at the indicated Q-values, are reported against the respective best fit lineshape (solid line). The additional, longitudinal, peak is also reported for comparison (dashed line)

Fig.9: In the left panel the parameters Γ_t (□) and Ω_t (•) measured in the liquid phase (T =295 K) are reported along with the corresponding quantities measured in the solid phase (dashed and solid lines, respectively). We also report for comparison the dispersion curves of single-crystalline D_2O (○) and H_2O (◊), as well as those of poly-crystalline H_2O (△). The $-\blacklozenge-$ data represent the measurement of the longitudinal branch of Ih measured by Criado et al.[55]. In the right panel we report the water Density of States, as evaluated by Incoherent Neutron Scattering in Ref. 57.

A Cunsolo et al. “Transverse dynamics of water across the melting: a parallel….”-Fig.1

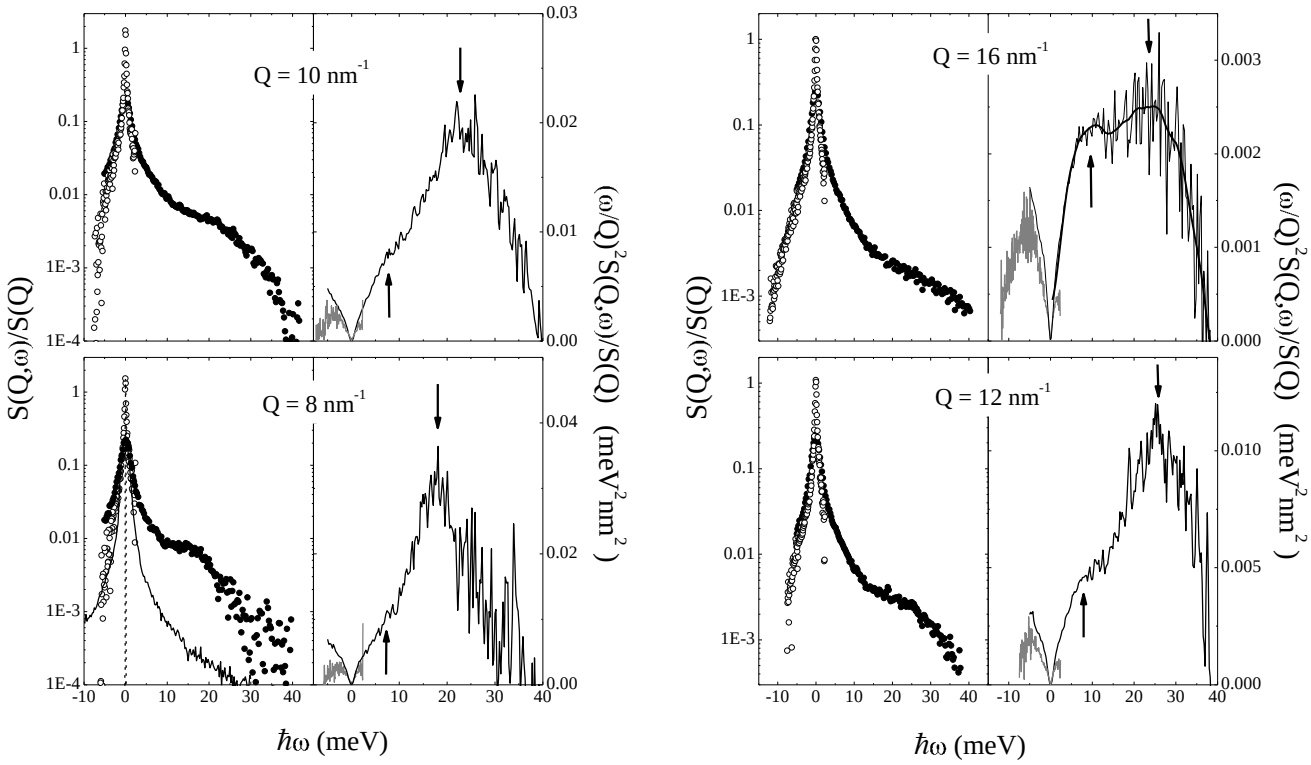

A Cunsolo et al. “Transverse dynamics of water across the melting: a parallel….”-Fig.2

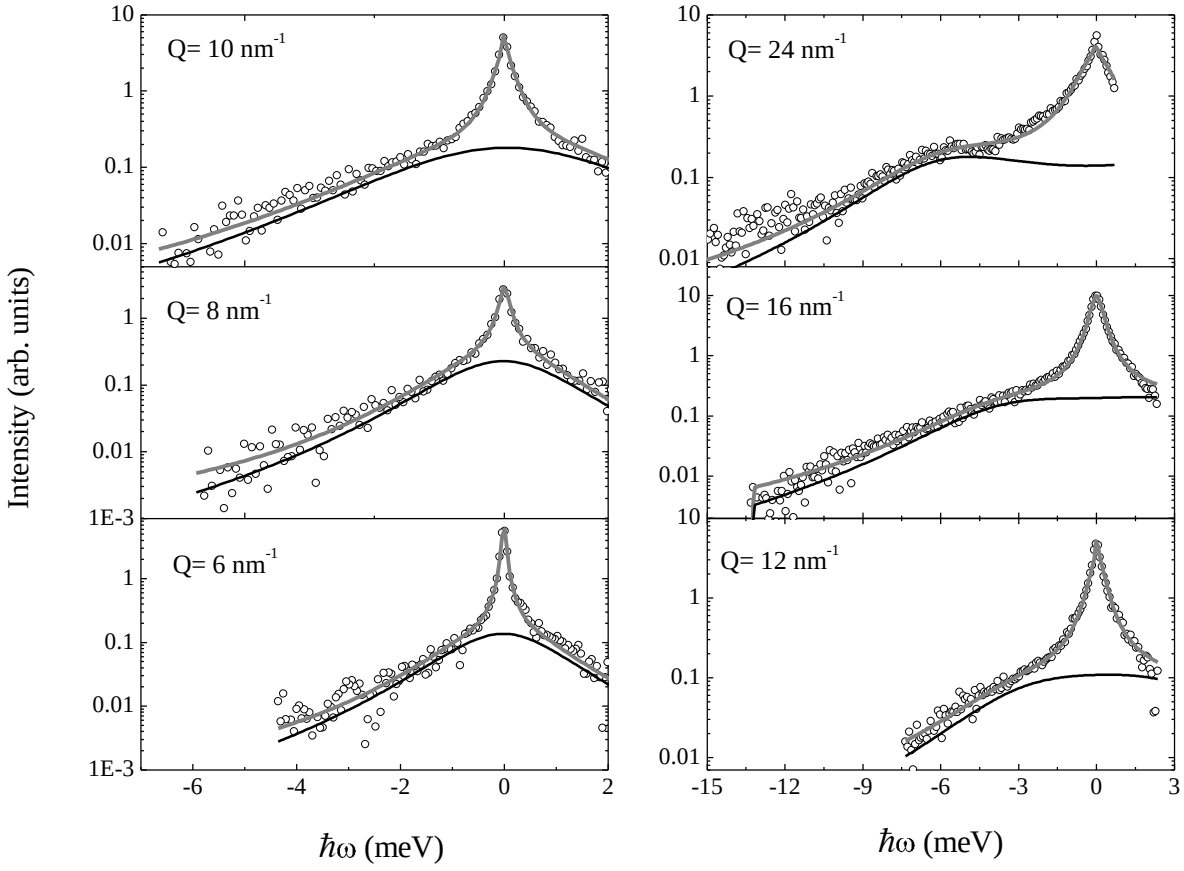

A Cunsolo et al. “Transverse dynamics of water across the melting: a parallel….”-Fig.3

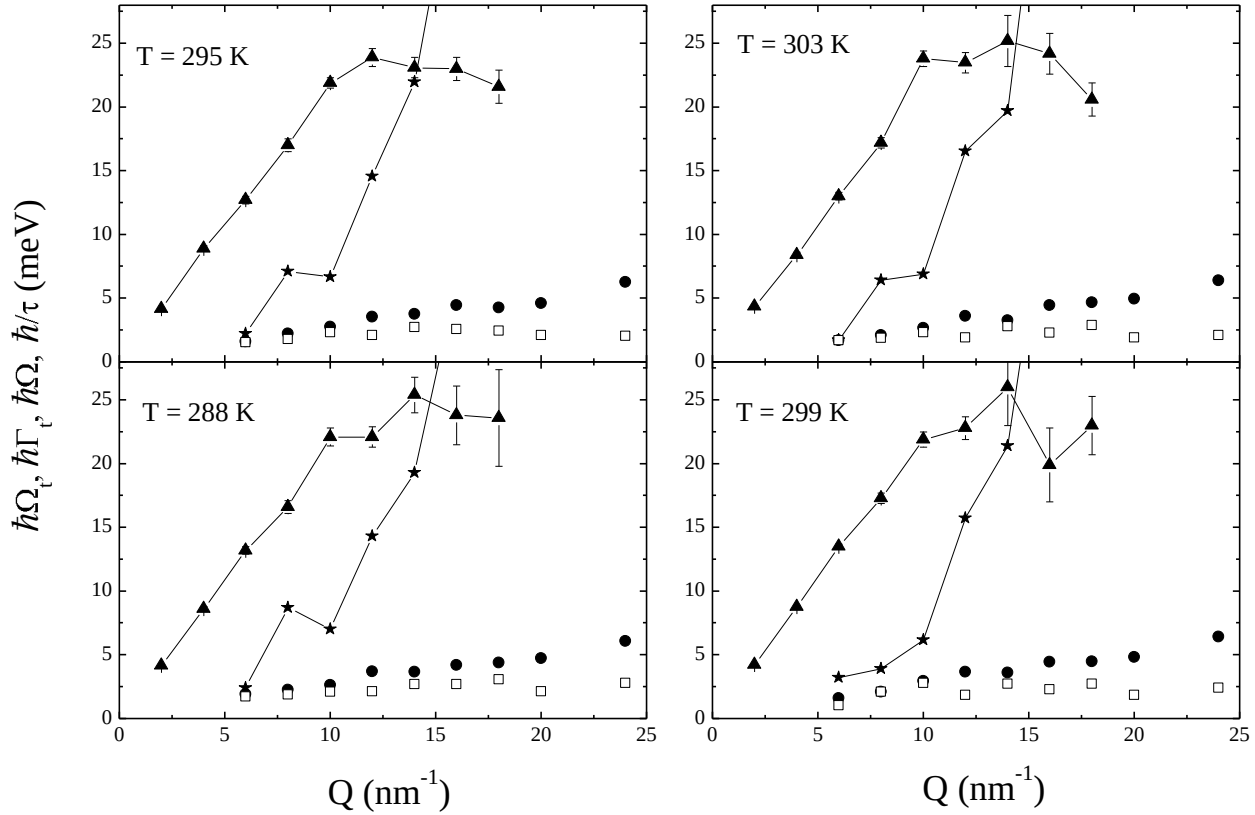

A Cunsolo et al. “Transverse dynamics of water across the melting: a parallel….”-Fig.4

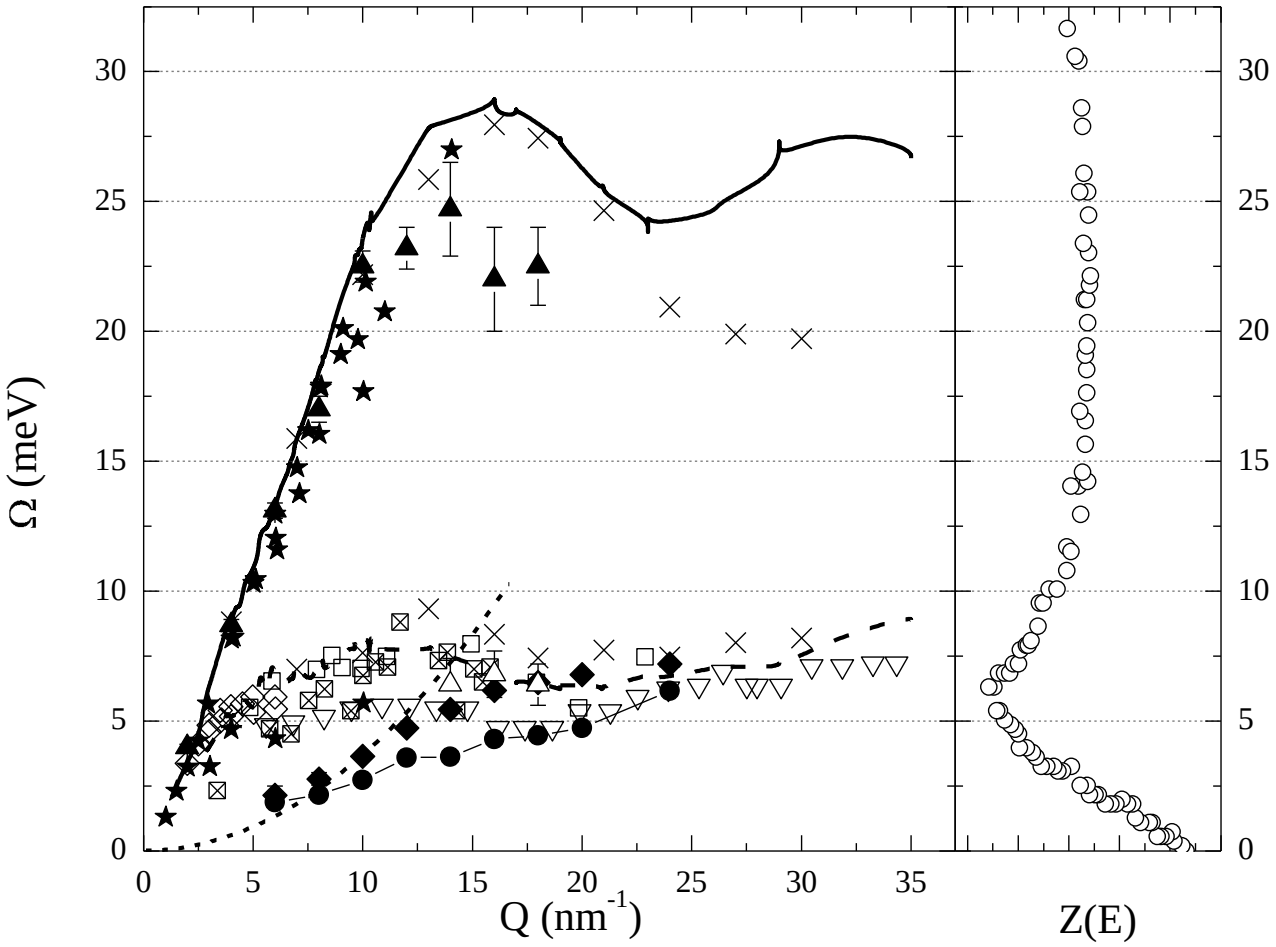

A Cunsolo et al. “Transverse dynamics of water across the melting: a parallel….”-Fig.5

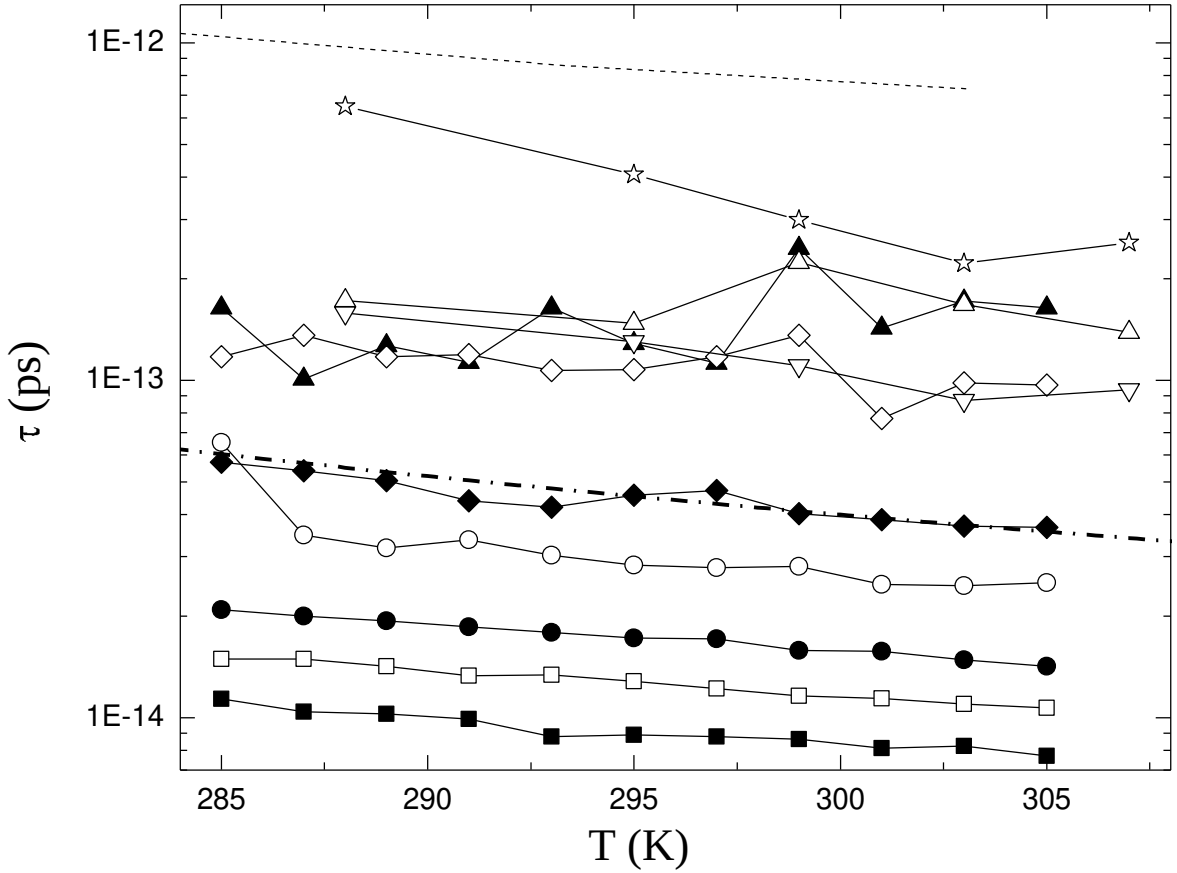

A Cunsolo et al. “Transverse dynamics of water across the melting: a parallel….”-Fig.6

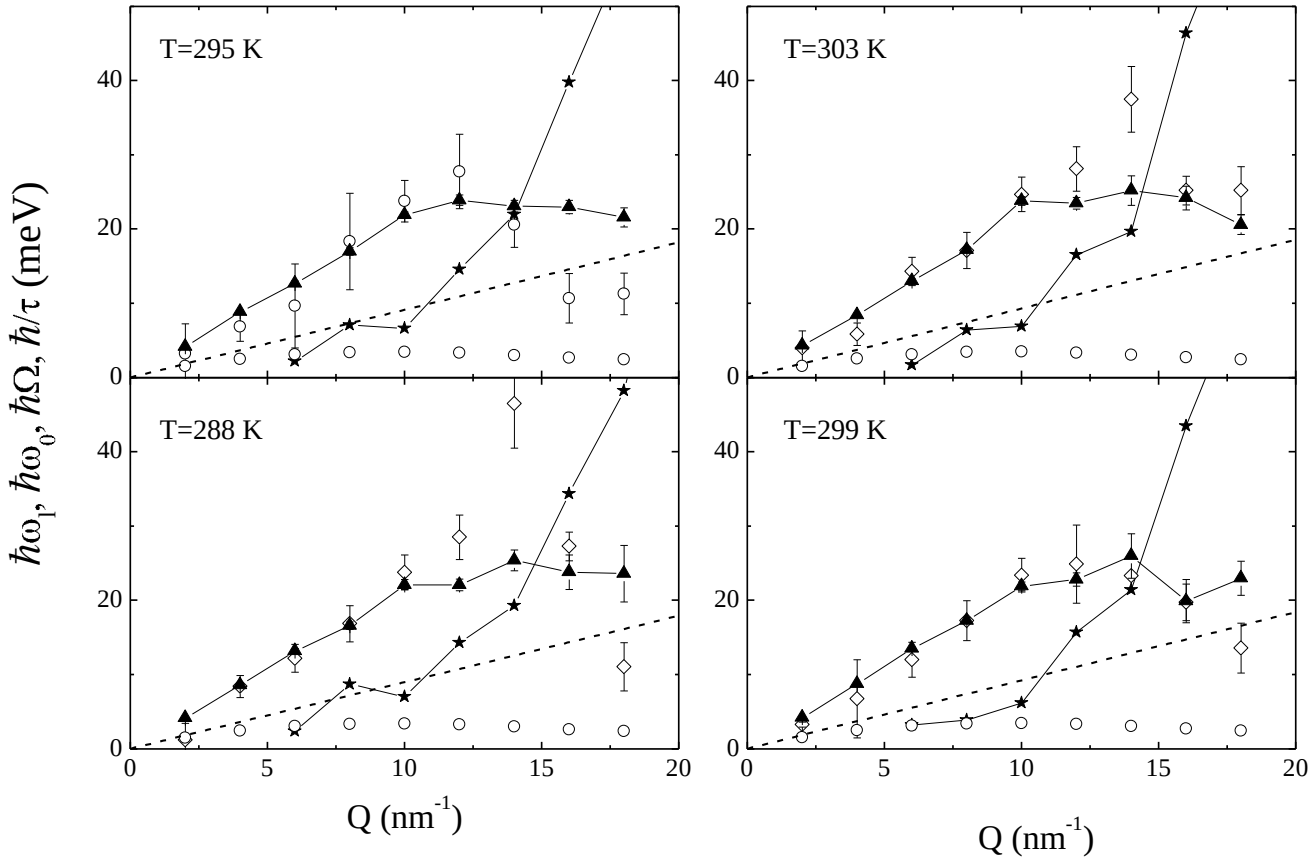

A Cunsolo et al. “Transverse dynamics of water across the melting: a parallel….”-Fig.7

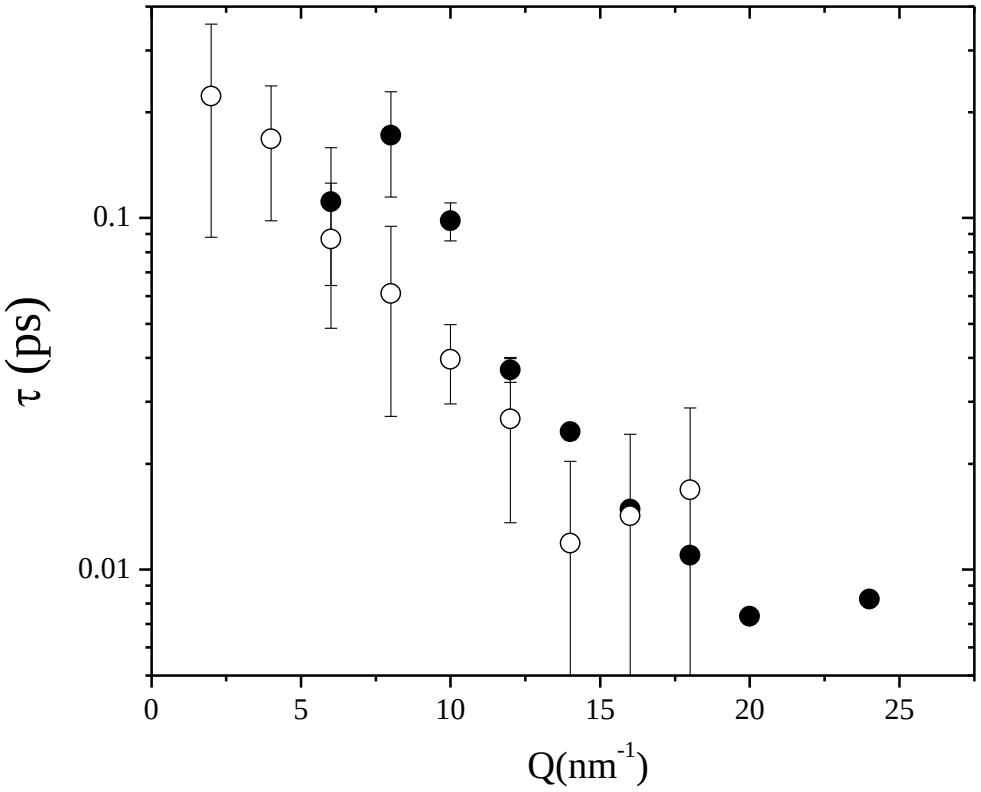

A Cunsolo et al. “Transverse dynamics of water across the melting: a parallel….”-Fig.8

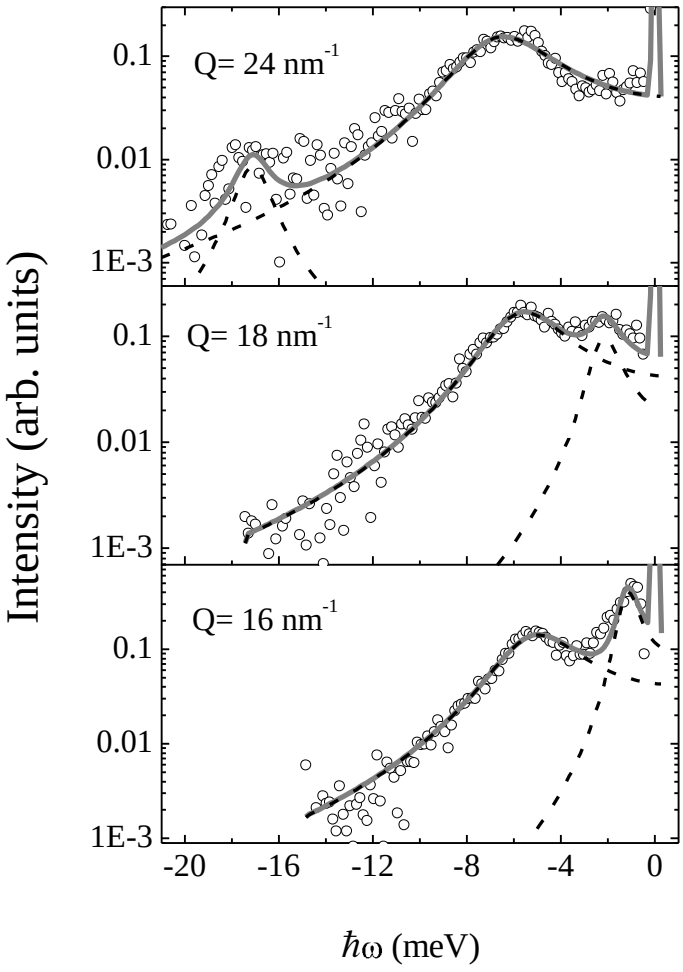

A Cunsolo et al. “Transverse dynamics of water across the melting: a parallel….”-Fig.9